

Shape Memory Alloy-based High Phase Order Motor

Claudio Rossi¹, Zongjian Yuan², Chao Zhang¹, Antonio Barrientos¹ and William Coral³

¹Centre for Automation and Robotics CAR UPM-CSCI, Madrid, Spain

²Northwestern Polytechnical University, Xi'an Shaanxi, China

³Universidad Politécnica de Madrid, Madrid, Spain

Keywords: Shape Memory Alloys, Stepper Motor, Artificial Muscles, Smart Materials, High Phase Order Motor.

Abstract: In this paper, we present our current work in the design and characterisation of a new shape memory alloy (SMA)-based High Phase Order Motor (HPOM). The motor can be used either in stepping mode or in servo mode of operation. Each phase of the motor consists of an SMA wire with a spring. The principle of operation of the HPOM is presented. In its operation the motor resembles a stepper motor though the actuation principles are different and hence has been characterised similar to a stepper motor. This motor can be actuated in either direction depending on which SMA is actuated, which are presented in this work. The motor is modelled and simulated and the results of simulations and experiments are presented.

1 INTRODUCTION

The Shape memory effect refers to the ability of certain materials to "remember" a determined shape at a specified temperature (Coral et al., 2012). Due to their unique behaviour, they are also called intelligent or smart material. Generally, NiTi (Nickel-Titanium) SMAs are the most common alloys used. NiTi SMAs work based on the shape memory effect, which essentially takes place by the influence of temperature. Heating this material by joule effect we obtain a contraction in the material, i.e. applying an electric current we can heat this material and thus produce movement. By definition, the electric resistivity is linked to the length of material, this means that the internal electrical resistance of the SMA changes when it contracts. Basically this allows us to use the SMA as an actuator and sensor simultaneously. In fact, most of the applications involving position linear control of SMAs, feedback electrical resistance measurements to estimate the motion generated by the actuator. This avoids the inclusion of external position sensors for closing the control loop.

Due to its characteristics compared to conventional technologies such as hydraulic/pneumatic actuators or electric motors/servomotors the SMAs offer improvements in the size, weight, strength, etc. for this reason in Robotics some applications have been developed using SMA (Rossi et al., 2010), (Rossi et al., 2011a) (Rossi et al., 2013), and (Colorado et al.,

2012). The actuators based on SMAs can be broadly classified into Limited Motion Type and Unlimited Motion Type. Under limited motion type both linear and rotary type actuators are presented in literature. Under unlimited motion type actuators only one type of motor was presented (Reynaerts and Brussel, 1998). This motor used springs made of SMA wires for actuation. Using SMA wire is possible to design actuator in tension mode (wire actuator), torsion mode (spring actuator) and bending mode (strip actuator), as presented by (Otsuka and Wayman, 1998) and (Reynaerts and Brussel, 1998). In terms of Energy Density the SMA actuator designed using SMA strips has 46 J/kg (Reynaerts and Brussel, 1998) while compared to SMA actuator designed using SMA wire has an energy density of 466 J/Kg. It is evident that the SMA used in tension mode has 100 times more energy density compared to SMA used in bending mode. Therefore, in this paper, we present our work to build a High Phase Order Motor, which uses SMA wires in tension mode. For the same volume of SMA material used the motor generates more torque compared to the motor designed with spring or strip type SMA actuator. It was noted (Kuribayashi, 1989) that SMA spring or strip generates force as a non-linear function of its deformed length. The actuation used in the present work generates a constant effective force throughout its operating range. The motor presented, works in stepping mode (Kuo and Tal, 1979), (Kuo, 1979) generating incremental motion and servo mode

generating continuous motion. The SMA wire based motor presented has better dynamic response compared to the motors that use SMA strips or springs. Analyzing the energy efficiency in the SMA actuator, it can never have a greater efficiency compared to a Carnot cycle between heating and cooling temperatures. Therefore, an SMA actuator will never compete directly with classical electric actuators. But the SMA has very high power to weight ratio and power to volume ratio compared to the conventional electric actuators and hydraulic actuators (Reynaerts and Brussel, 1998). There are several applications where the energy efficiency is not significant but a large power has to be generated with a compact size and light weight actuator. Therefore, SMA has found wide usage in Space, Robotics and Medical application due to its compact size, light weight, extremely cheap, capable of working at low voltages, easily available commercially¹ non magnetic property, large force-weight ratio, large life cycles, negligible volume, sensing capability, noise-free operation, smooth and insensitivity to space radiations, namely, electrons, protons and heavy ions. The experience gained during the last years at the Bioinspired Systems Lab² of CAR UPM-CSIC with previously designed robots has demonstrated that by (i) finding suitable niches of application, (ii) dedicated mechatronics design, and (iii) ad-hoc control strategies, SMAs can effectively be used as an alternative actuation technology in a wide spectrum of applications and robotic systems.

2 MECHANICAL DESIGN

Following the same principle of a conventional electric motor, the proposed actuator is composed of two parts, stator and rotor. Here, the stator and the rotor are called, respectively, break and plate. Both parts of the actuator have been prototyped in ABS and produced with a 3D Printer. Three groups of SMA work on the actuator. We name them as group A, B, C (see Figures 2 and 4). All SMAs adopted have a diameter of $150\mu\text{m}$, a pull force of 321 grams-force, a power consumption of 410mA at room temperature, and a nominal contraction time of 1 second. Note that contraction time can be improved by overloading (Rossi et al., 2010). The diameter size of the SMA wires has been chosen as a trade-off between current consumption, pull force and contraction time.

¹NiTi (Nickel-Titanium), such as NiTiInol[®] are the most commonly commercially available SMAs.

²http://www.disam.upm.es/~crossi/Bio_Inspired_Robots/Bio_Home.html.

2.1 Brake

Is composed by two identical arms, each facing each other. The figure 1 shows the Top and Bottom view in one of this arms. This part moves the shaft in both directions (clockwise and counterclockwise) or block and prevent undesirable movements. Both functions by grasping the shaft between the Shaft Hole. This functions are achieved by controlling the contraction of the SMAs located within the two brake arms as show in the figure 2.

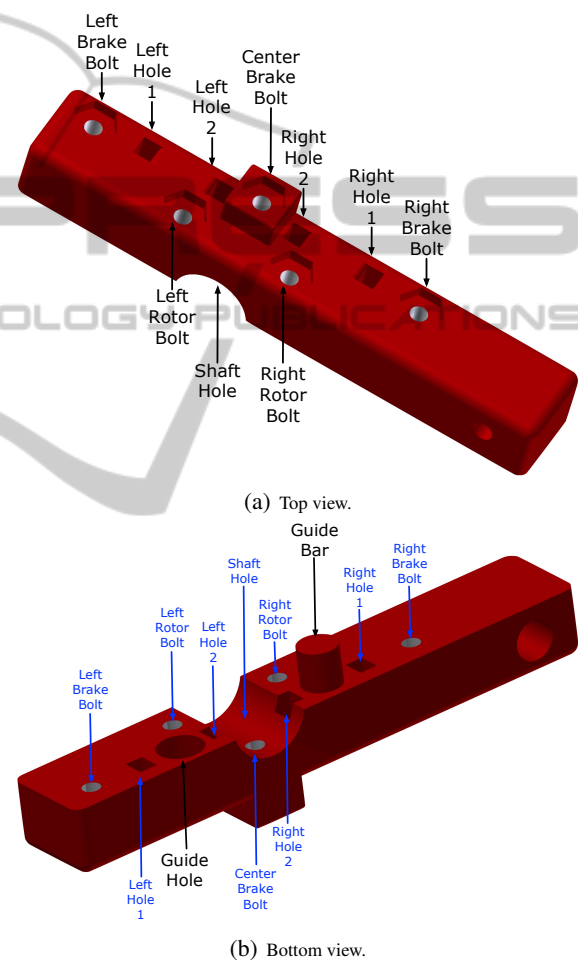


Figure 1: Break arms.

There are two pairs of SMA wires called Group C that can be actuated by separate or at same time to increase the amount of forces applied to the shaft. Each of these connect the two arms in two sections and 8 Points. In this way the force to grasp the shaft is multiplied by four times the force of the SMA. The force diagram is show in the figure 3 and it is represented in the equations below.

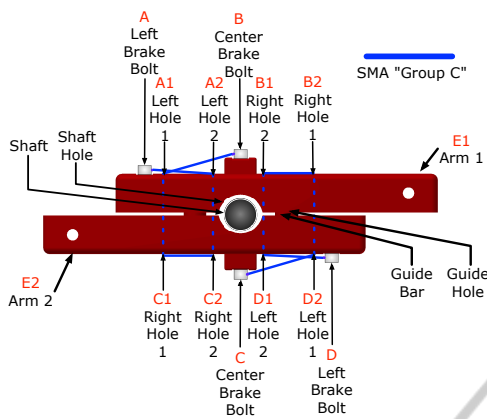


Figure 2: Arrangement of the SMA wires actuating the brake.

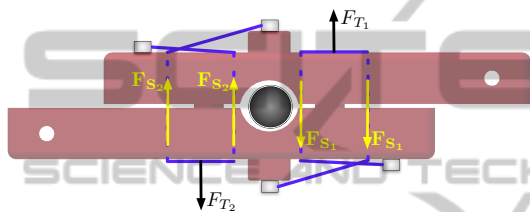


Figure 3: Forces acting on the brake.

$$F_{T1} = F_{S1} + F_{S1}$$

$$F_{S1} = \frac{1}{2} F_{SMA1}$$

$$F_{T1} = F_{SMA1} \tag{1}$$

$$F_{T2} = F_{SMA2} \tag{2}$$

$$F_{SMA1} = F_{SMA2}$$

$$F_T = F_{T1} + F_{T2} \tag{3}$$

2.2 Plate

This is the base where the brake is housed. Is composed by only one part. The most function of this part is to houses the SMAs that allow to rotate the brake, that will act as a rotor. The radius of the plate is set in such a way to allow arranging a large segment of the SMAs, which is passes through set of guides. Such arrangement, shown in Figure 4 is needed since the SMA wires only contracts approximately a 4% of their length, and this group of SMAs determines the number of degrees that the brake can rotate. The speed and the amount of rotation over the brake is determined controlling the contraction of the SMAs. Two pairs of SMA wires that can be actuated individually or at same time depending of the amount of force to be applied to the brake to rotate the shaft (when it is blocking it) and how much force is to be applied.

The Group A allows to rotate the brake clockwise and the Group B counterclockwise. Each phase is composed by one "Group A and B" the Figure 4a show only one phase. Each time that another phase is required (for improved speed) we only need to add other plate more like in a sandwich. Note that at rest position SMAs A are fully extended, while SMAs B are loose, in such a way not to prevent SMAs A to contract. When SMAs A are contracted, SMAs B will be fully extended and thus ready to contract to bring the brake back to the start position.

The force applied to the brake to rotate it for every wire is 321 grams-force this because the friction between the SMA and the screw is negligible.

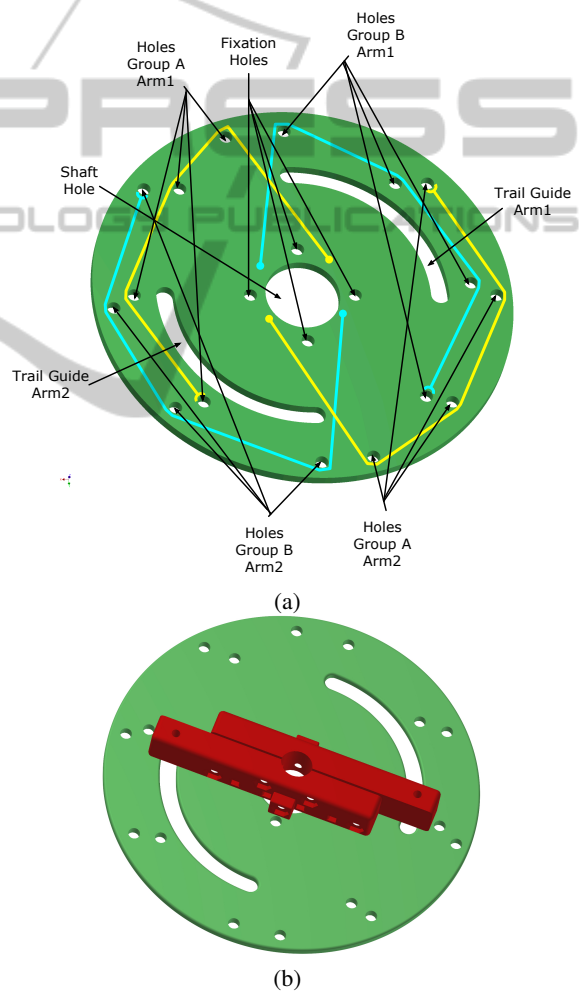


Figure 4: Arrangement of the SMA wires used to rotate the brake (a) and arrangement of the two parts (b).

3 OPERATION PRINCIPLE

3.1 Principle of One Way Shape Memory Effect

The ability to remember a predetermined shape after several deformation is called Shape Memory Effect (SME). The Martensite phase transformation is responsible for the shape changes with temperature variation. Commonly SMA wires are made of metal alloys (nickel-titanium) and they are known as NiTi. The NiTi alloy is trained to remember a short length at high temperature by heat treatment. In cold state (Martensite) the SMA is malleable and can be stretched to a longer length with a small force. Normally in SMA actuators a biasing force is applied during the cold condition to stretch the SMA wire to a designed length faster. this process is known as pre-loading. Pre-loading is usually done by using a spring in series with the SMA wire or a weight (W) to generate force by gravity (figure5). When the SMA is heated to high temperature (Austenite), SMA shrinks to the trained length. While shrinking, the SMA becomes hard, and can pull much larger force than what is required to stretch SMA at low temperature. The proposed High Phase Order motor is designed using one way SMA wires.

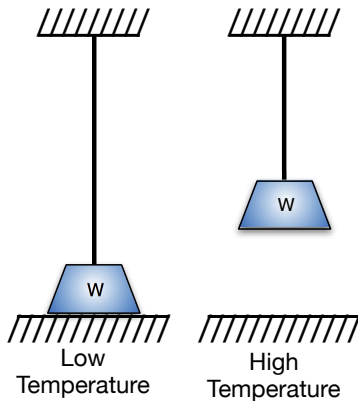


Figure 5: One way SMA actuation.

3.2 Shape Memory Alloy-Based HPOM Operating Principle

The principle of functioning can be explained in 5 steps (always actuating the SMA Groups A, B, and C) as shown below.

- **Step 1:** The "Group C" (phase 1) is actuated and the shaft is locked.

- **Step 2:** While the "Group C" (phase 1) is actuated, the "Group A or B" (phase 1) (depending on the way of rotation, clockwise or counterclockwise) is actuated simultaneously. To simplify the explanation we decided to actuate the "Group A"
- **Step 3:** When the "Group A" (phase 1) is fully contracted we release it and the "Group C" from the phase 2 is actuated.
- **Step 4:** The "Group C" (phase 1) is released and the "Group A" (phase 2) is actuated.
- **Step 5:** When the "Group A" (phase 2) is fully contracted we release it and the "Group C" from the phase 2 is released.

4 MODELING AND CONTROL

Both parts (brake and plate) are controlled with a PID controller with an external force feedback loop control. Using the changes over the internal resistance of the SMA it is possible to implement as well a position control. Force/position control strategies provide an effective framework to deal with tasks involving interaction with the environment.

4.1 System Identification and Controller

Using the force feedback loop we can linearize the behaviour of the SMA. In this way we obtain experimentally the model for the brake and plate. The input signal used to actuate the SMA and the output signal obtained by the force sensor due to this action is shown in the Figure 6. After system identification, carried out using the "ident" tool box of MATLAB®, the transfer function obtained is:

$$G(s) = \frac{0.002697s + 0.0001736}{s^2 + 0.02438s + 0.003559}$$

The step response of $G(s)$ in open loop is shown in Figure 7.

For the control, we used a PID (proportional-integral-derivative) controller, which responds to the equation:

$$u(t) = K_p e(t) + K_i \int_0^t e(t) dt + K_d \frac{de(t)}{dt}, \quad (4)$$

where $e(t)$ is the signal error and $u(t)$ is the control input of the process. K_p, K_i, K_e are the proportional, integrative and derivative gains. We have tuned the values to the three parameters (K_p, K_i, K_d) of the PID controller based on the analysis of the open and close

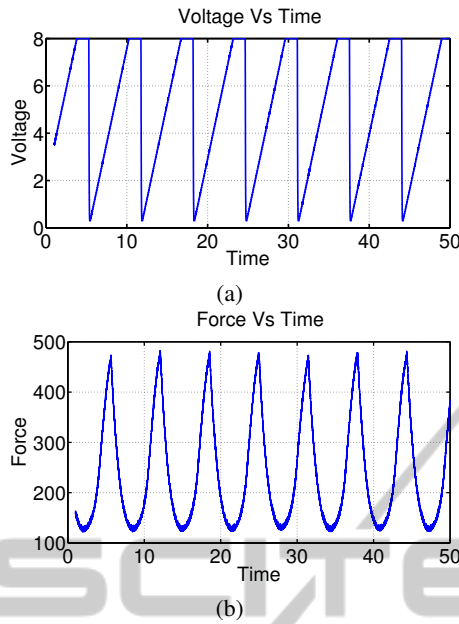


Figure 6: SMA step response in open loop (a) Input, Voltage (V) Vs Time (s), (b) Output, Force (gf) Vs Time (s).

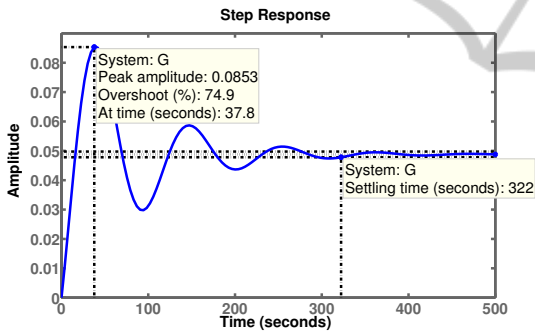


Figure 7: G(s) Step response in open loop.

loop of the system to be controlled. The PID controller gains obtained are:

$$K_p = 50000, \quad K_i = 1000, \quad K_d = 100$$

and the transfer function including the PID controller and the feedback is:

$$GLC3(s) = \frac{2.697s^3 + 135s^2 + 8.95s + 0.01736}{3.697s^3 + 135s^2 + 8.953s + 0.01736}$$

Figure 8. shows the step response of function $GLC3(s)$.

4.2 Control Schema

In the control system (Fig. 9), the force error is converted in a suitable reference trajectory for the inner position controller which is defined in the Cartesian space or the angular space (De Schutter and van Brussel, 1988). When there are no constraints due to the

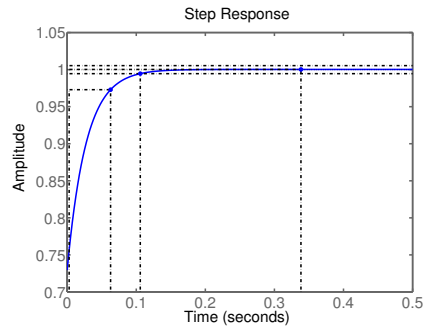


Figure 8: Step response function $GLC3(s)$. Peak Response 0.338s, Settling Time 0.106s, Rise Time 0.06s.

environment, the force controller will be without effect and the position controller will continue to control the system. When constraints appear, the force controller allows the control of the generated efforts. This configuration makes it possible to control the force and the position simultaneously. The force control loop is designed to prevail over the position control loop the event of a conflict (Ferguene and Redouane, 2009). This means that the force controller dominates the position controller

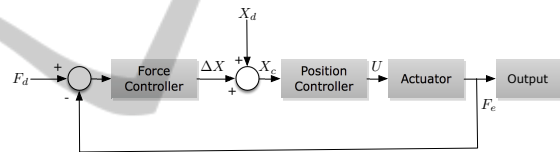


Figure 9: Control schema (X_d : Desired Position; F_d : Desired Force; ΔX : Modifier resulting from the force control loop; X_c : Position command; U : Control Reference; F_e : Environment Force).

5 EXPERIMENTAL RESULTS

This section primarily describes the experimental tests, along with a comparison of the results with theoretical predictions. The experimental tests were performed at different excitation frequencies but same amplitude while keeping the same input signal (sine wave)

The experimental setup for the system identification was made using the Control Electronic Circuit (CEC) (Rossi et al., 2010), (Rossi et al., 2011a), (Rossi et al., 2011b). Its allows to measure voltages and current through the SMA wires as well as to program the PIC microcontroller embedded on the circuit to directly control the SMA without external devices. It is also possible to communicate with this through the I2C Bus, SPI Bus or Serial Port. Using the voltage and current we can estimate the value and the changes

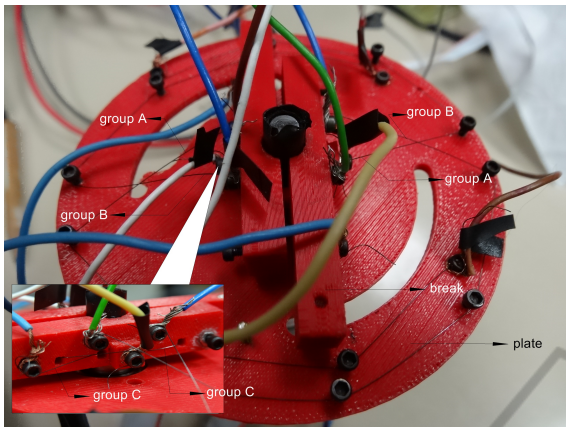


Figure 10: Experimental testbed, Plate and Brake.

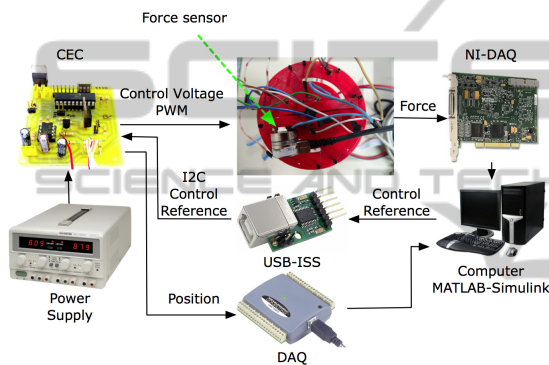
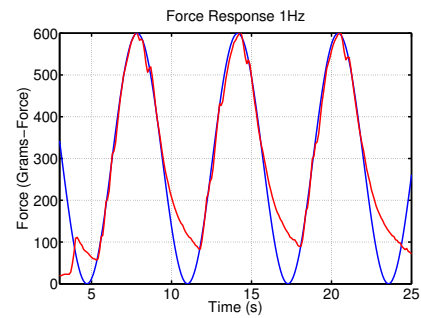


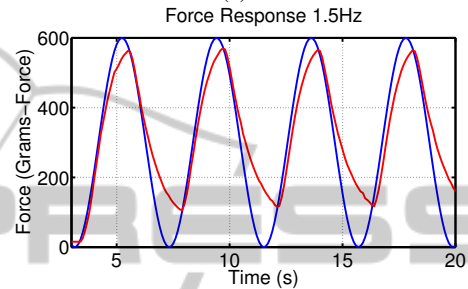
Figure 11: Experimental testbed.

over the internal resistance in the SMA and is possible in this way to know the actual percentage of shrinking. The method consists in measuring the electrical resistance of an SMA element (Teh and Featherstone, 2008), calculating a maximum safe heating current as a function of measured resistance, and ensuring that the actual heating current does not exceed this maximum value. In fact resistance is being used as a form of temperature measurement, and the maximum safe heating current is designed to prevent overheating. The force response is measured using a Nano 17 transducer (ATI Industrial Automation,) through a data acquisition card (NI-DAQ) NI PCI-6220 (Nation Instruments,). It has a 0.318 gram-force of resolution. The figure 10 shows the testbed used. This also shows the data acquisition device (DAQ) USB-1208FS (Measurement Computing,) used to measure the voltages from the CEC and the USB-ISS allows communication between the Computer and CEC through I2C Bus. The complete setup is depicted in figure 11.

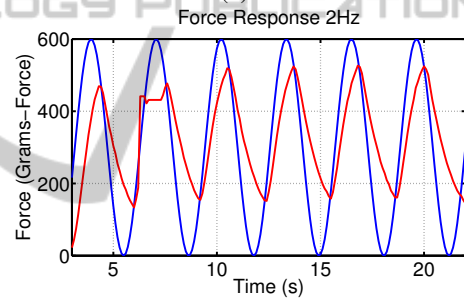
When the frequency increase the tracking error also increases but increasing the *ISMA* the speed response improves. In this way the tracking error is re-



(a)



(b)



(c)

Figure 12: Experimental results: (a) Force response at 1 Hz, (b) 1.5 Hz, (c) 2 Hz.

duced. Theoretically the maximum force produced from the SMA in the Group A was 642 grams-force experimentally we obtained a force (frequency 1 Hz) of 600 grams-force.

6 CONCLUSIONS

In this study we built and characterised a novel actuator based in Shape Memory Alloy (SMA) wires. The actuator can be instrumented to measure input power and output force and SMA electric resistance for a wide variety of force inputs and actuation speeds. Because each of the force inputs are replicable, the actuator can be actuated with thousands of combinations of force parameters while providing valuable data on force and power. The broad range of capabilities of this actuator make it an excellent tool to be

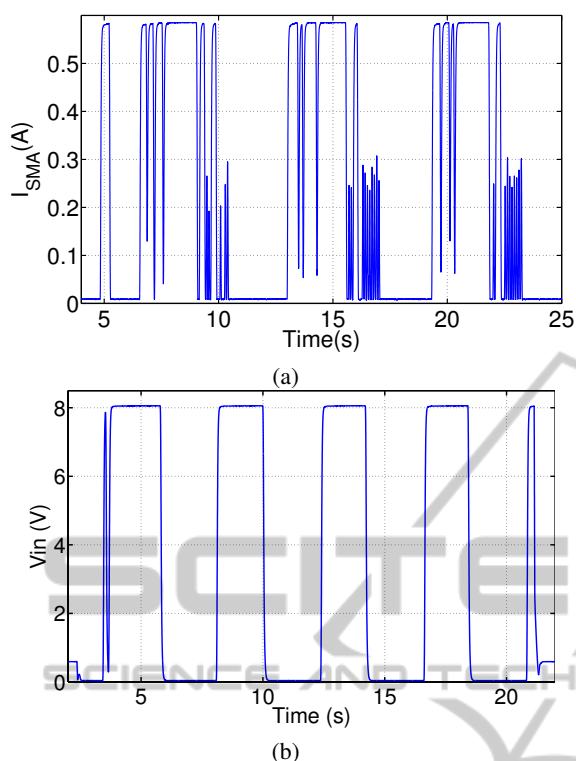


Figure 13: Experimental results: (a) ISMA (A) Vs Time (s) at 1 Hz, (b) Vin (V) Vs Time (s) at 1.5 Hz.

used like a stepper motor (because we can control the contraction length and have resolution of steps from less than a millimeter) or continuous motor in applications where the weight a size are critical, and in particular to make less complex robots reducing the control and hardware cost.

ACKNOWLEDGEMENTS

William Coral acknowledge to the Administrative Department of Science, Technology and Innovation (COLCIENCIAS) (grant call 568 2013) and COLFUTURO (grant call 2012) from Colombia for its support. The authors acknowledge the support of the Robotics and Cybernetics Group at the Centre for Automation and Robotics UPM-CSIC, the project ROBOCITY 2030 (Community of Madrid S-0505/DPI/000235) and the project ROTOS (Ministry of Science And Innovation of Spain DPI2010-17998).

REFERENCES

ATI Industrial Automation. F/T Sensor: Nano17. <http://www.ati-ia.com>. Accessed June 6, 2013.

- Colorado, J., Barrientos, A., and Rossi, C. (2012). Biomechanics of smart wings in a bat robot: morphing wings using SMA actuators. *Bioinspiration & Biomimetics*.
- Coral, W., Rossi, C., and Montano, J. C. (2012). SMA-Based Muscle-Like Actuation in Biologically Inspired Robots: A State of the Art Review. page 30. INTECH.
- De Schutter, J. and van Brussel, H. (1988). Compliant robot motion ii. a control approach based on external control loops. *International Journal of Robotics Research*, 7(4):18–33.
- Ferguene, Farid, T. and Redouane (2009). Dynamic external force feedback loop control of a robot manipulator using a neural compensator, application to the trajectory following in an unknown environment. *International Journal of Applied Mathematics and Computer Science*, 19(1):113–126.
- Kuo, B. C. (1979). *Step motors and control systems*. Incremental motion control, SRL Pub. Co.
- Kuo, B. C. and Tal, J. (1979). *Incremental Motion Control: Step motors and control systems*, edited by B. C. Kuo. Incremental Motion Control. SRL Publishing Company.
- Kuribayashi, K. (1989). A new servo motor using shape memory alloy. In *Industrial Electronics Society, 1989. IECON '89., 15th Annual Conference of IEEE*, pages 139–144 and 238–243.
- Measurement Computing. USB-1208FS. <http://www.mccdaq.com/usb-data-acquisition/USB-1208FS.aspx>. Accessed June 6, 2013.
- Nation Instruments. NI PCI-6220. <http://sine.ni.com/nips/cds/view/p/lang/es/nid/14130>. Accessed June 6, 2013.
- Otsuka, K. and Wayman, C. M. (1998). Mechanism of shape memory effect and superelasticity. *Shape memory materials*.
- Reynaerts, D. and Brussel, H. V. (1998). Design aspects of shape memory actuators. *Mechatronics*, 8(6):635–656.
- Rossi, C., Colorado, J., Coral, W., and Barrientos, A. (2011a). Bending continuous structures with SMAs: a novel robotic fish design. *Bioinspiration & Biomimetics*, 6(4):045005.
- Rossi, C., Coral, W., and Barrientos, A. (2010). SMA Control for Bio-mimetic Fish Locomotion. In *International Conference on Informatics in Control, Automation and Robotics (ICINCO)*, Madeira.
- Rossi, C., Coral, W., and Barrientos, A. (2013). Robotic Fish to Lead the School. In Palstra, A. P. and Planas, J. V., editors, *Swimming Physiology of Fish*, pages 407–421. Springer Berlin Heidelberg.
- Rossi, C., Coral, W., Colorado, J., and Barrientos, A. (2011b). A motor-less and gear-less bio-mimetic robotic fish design. In *Robotics and Automation (ICRA), 2011 IEEE International Conference on*, pages 3646–3651.
- Teh, Y. H. and Featherstone, R. (2008). An architecture for fast and accurate control of shape memory alloy actuators. *International Journal of Robotics Research*, 27(5):595–611.